HHS Public Access

Author manuscript

Mol Cancer Ther. Author manuscript; available in PMC 2019 October 01.

Published in final edited form as:

Mol Cancer Ther. 2018 October ; 17(10): 2112–2122. doi:10.1158/1535-7163.MCT-17-0131.

Cabozantinib exhibits potent antitumor activity in colorectal cancer patient-derived tumor xenograft models via autophagy and signaling mechanisms

Aaron J Scott[1], **Stacey M Bagby**[2], **Rachel Yahn**[2], **Kendra M Huber**[3], **Natalie J Serkova**[3], **Anna Nguyen**[2], **Jihye Kim**[2], **Andrew Thorburn**[4], **Jon Vogel**[5], **Kevin S. Quackenbush**[2], **Anna Capasso**[2], **Anna Schreiber**[2], **Patrick Blatchford**[2], **Peter J Klauck**[2], **Todd M. Pitts**[2], **S. Gail Eckhardt**[6,*], and **Wells Messersmith**[2]

[1]Division of Hematology and Oncology, Banner University of Arizona Cancer Center, Tucson, AZ

[2]Division of Medical Oncology, University of Colorado Anschutz Medical Campus and University of Colorado Cancer Center, Aurora, CO

[3]Department of Anesthesia, University of Colorado Anschutz Medical Campus and University of Colorado Cancer Center, Aurora, CO

[4]Department of Pharmacology, University of Colorado Anschutz Medical Campus and University of Colorado Cancer Center, Aurora, CO

[5]Department of Surgery, University of Colorado Anschutz Medical Campus and University of Colorado Cancer Center, Aurora, CO

[6]Division of Medical Oncology, The University of Texas at Austin, Austin, TX

Abstract

Anti-angiogenic therapy used in treatment of metastatic colorectal cancer (mCRC) inevitably succumbs to treatment resistance. Upregulation of MET may play an essential role to acquired anti-VEGF resistance. We previously reported that cabozantinib (XL184), an inhibitor of receptor tyrosine kinases (RTKs) including MET, AXL, and VEGFR2, had potent antitumor effects in mCRC patient-derived tumor explant models. In this study, we examined the mechanisms of cabozantinib sensitivity, using regorafenib as a control. The tumor growth inhibition index (TGII) was used to compare treatment effects of cabozantinib 30mg/kg daily versus regorafenib 10mg/kg daily for a maximum of 28 days in 10 PDX mouse models. *In vivo* angiogenesis and glucose uptake were assessed using dynamic contrast-enhanced (DCE)-MRI and [^{18}F]-FDG-PET imaging, respectively. RNA Seq, RTK assay, and immunoblotting analysis were used to evaluate gene pathway regulation *in vivo* and *in vitro*. Analysis of TGII demonstrated significant antitumor effects with cabozantinib compared to regorafenib (average TGII 3.202 versus 48.48, respectively; P = 0.007). Cabozantinib significantly reduced vascularity and glucose uptake compared to

[*]Current Address: S. Gail Eckhardt, M.D. FASCO, Dell Medical School | The University of Texas at Austin, Chair, Department of Oncology, CPRIT Scholar, Professor and Associate Dean of Cancer Programs, Austin, Texas. **Corresponding Author:** Aaron J Scott, 1515 N Campbell Ave, Rm 1916, Tucson, AZ 85724, ajscott@email.arizona.edu; office phone: (520) 626-2224; fax: (520) 626-2225.

Conflict of interest disclosure statement:
Authors report no conflicts of interest.

baseline. Gene pathway analysis showed that cabozantinib significantly decreased protein activity involved in glycolysis and upregulated proteins involved in autophagy compared to control, whereas regorafenib did not. The combination of two separate anti-autophagy agents, SBI-0206965 and chloroquine, plus cabozantinib increased apoptosis *in vitro*. Cabozantinib demonstrated significant antitumor activity, reduction in tumor vascularity, increased autophagy, and altered cell metabolism compared to regorafenib. Our findings support further evaluation of cabozantinib and combinational approaches targeting autophagy in CRC.

Keywords

Cabozantinib; MET; VEGF; angiogenesis; autophagy

Introduction

Colorectal cancer (CRC) is the third most common cancer diagnosed annually in the United States (1). Metastatic CRC (mCRC) is the second leading cause of cancer-related death with an estimated 50,000 deaths in the United States and over 500,000 deaths worldwide annually (1). Despite substantial improvements in treatment over the past decade, mCRC carries a poor prognosis with a median overall survival of roughly 30 months with optimal combination chemotherapy. While regorafenib has been approved for refractory mCRC, the benefit of this therapy is modest at best with a median overall survival benefit of 1.4 months compared to best supportive care (2, 3). Unfortunately, resistance to regorafenib occurs quickly for most individuals.

Expression of vascular endothelial growth factor (VEGF) and its receptors, VEGFR1 and VEGFR2, has been shown to be upregulated in many tumor types. VEGF ligand binding and activation of VEGFR2 is likely the major driver of tumor neovascularization (4). Regorafenib, a multikinase inhibitor targeting VEGFR2, KIT, RET, TIE2, BRAF, and PDGFR, has received FDA approval for treatment of refractory mCRC. The inhibition of VEGFR2 by regorafenib is thought to be a central mechanism for its activity in treatment of mCRC. In addition to regorafenib, three other anti-angiogenic agents have received FDA approval in combination with chemotherapy to treat mCRC: bevacizumab, a monoclonal antibody targeting VEGF; ziv-aflibercept, a recombinant fusion protein decoy receptor of VEGFR1 and 2; and ramucirumab, a monoclonal antibody targeting VEGFR2. These agents add incremental benefit in progression-free survival and overall survival compared to chemotherapy alone in mCRC (5).

Treatment with anti-angiogenics is often short-lived due to development of acquired resistance. Previously published data have shown that the MET kinase pathway promotes resistance to anti-angiogenic therapy (6–8). The RTK MET, also known as the hepatocyte growth factor receptor (HGFR), has been classified as a proto-oncogene that drives tumor cell survival, metastasis, and resistance to anti-cancer therapies (9). MET expression alone has correlated with worse prognosis, tumor invasion, and lymph node invasion in CRC (10). In addition, evidence from multiple preclinical studies has demonstrated that MET and VEGF receptor pathways may cooperate to promote tumor angiogenesis and provides a

mechanism for resistance to selective blockade of either pathway (11–13). Increased MET activation also allows cancer cells to undergo epithelial-mesenchymal transition (EMT), facilitating cell metastases to less hypoxic conditions and a more favourable environment for cell survival (14, 15). Due to this, interest in inhibiting the VEGF and MET axes for treatment in a variety of malignancies continues to grow.

Cabozantinib (XL184) is an orally-bioavailable, small-molecule inhibitor of multiple kinases central to cancer cell growth, angiogenesis, and metabolism including VEGFR2/KDR, MET, AXL, RET, TIE2, and KIT. While the kinase target profile of regorafenib is similar, it does not inhibit MET. Cabozantinib has demonstrated activity in multiple tumor types and has received FDA approval for treatment of previously-treated metastatic renal cell carcinoma and metastatic medullary thyroid cancer (16, 17). Previously we demonstrated that treatment of CRC patient-derived xenografts (PDX) with cabozantinib led to potent inhibition of tumor growth in 80% of treated tumors in CRC explant models (18). The conclusion was that the dual inhibition of MET and VEGFR2 is central to the anti-tumor effects of cabozantinib.

In this study, we aimed to investigate mechanisms of the anti-tumor effects of cabozantinib in colorectal cancer PDX models, using regorafenib as a comparator. We hypothesized that anti-tumor activity of cabozantinib would be superior to regorafenib in CRC PDX models due to dual inhibition of MET and VEGFR2, as well as potentially other metabolic and autophagy mechanisms.

Materials and Methods

CRC Patient Derived Xenograft Model.

Patient-derived tumor tissues were acquired from the University of Colorado Hospital. All patients consented their tissue to be used in in the study in accordance with protocols approved by the Colorado Multiple Institutional Review Board. Female athymic nude mice ages four to eight weeks of age were purchased from Envigo (Washington DC). All animal experiments for this study were approved by the Institutional Animal Care and Use Committee. Tumor specimens obtained from pathology were finely minced and implanted in mice and passed into subsequent generations (19). For treatment studies involving cabozantinib and regorafenib, tumors were expanded subcutaneously in the left and right flanks of mice (≥ 10 tumors/group) and randomized into groups receiving vehicle, cabozantinib (30 mg/kg) or regorafenib (10 mg/kg) according to published studies (18, 20–22). Treatment started when the average tumor volumes reached ~ 200 mm^3. Mice were treated with vehicle (no drug), cabozantinib, or regorafenib for 28 days. Mice were monitored daily for signs of toxicity and tumor size was evaluated twice per week by calliper measurements using the following formula: tumor volume = [length × $width^2$] * 0.52.

MET Kinase Active HCT116 cell line xenograft model.

The HCT116 MET kinase active Y1253D and HCT116 (control) isogenic CRC cell lines were obtained from Horizon (Cambridge, MA, USA). Cells were cultured in RPMI media

containing 10% fetal bovine serum, 1% non-essential amino acids, and 1% penicillin/streptomycin. The MET kinase active and HCT116 isogenic cell lines were harvested, washed with complete media and resuspended 50% media and 50% matrigel. One million cells in a volume of 100 μl were injected subcutaneously in both flanks of each mouse (≥ 10 tumors/group). Mice were randomized into groups receiving vehicle, cabozantinib (30 mg/kg) or regorafenib (10 mg/kg). Treatment started when the average tumor volumes reached ~ 200 mm^3. Mice were monitored daily for signs of toxicity and tumor size was evaluated twice per week by calliper measurements using the following formula: tumor volume = [length × $width^2$] * 0.52.

Human colorectal cancer cell lines were obtained from ATCC (Manassas, VA, USA), DSMZ Cell Line Bank (Braunschweig, Germany), ECACC (Sigma, St. Louis, MO) and the Korean Cell Line Bank (KCLB) (Seoul, South Korea). The GEO cell line was a generous gift from Dr. Fortunato Ciardiello (Cattedra di Oncologia Medica, Dipartimento Medico-Chirurgico di Internistica Clinica e Sperimentale “F Magrassi e A Lanzara,” Seconda Università degli Studi di Napoli, Naples, Italy). All cell lines were cultured in RPMI media supplemented with 10% fetal bovine serum, 1% penicillin-streptomycin and 1% MEM nonessential amino acids and routinely screened for the presence of mycoplasma (Mycoplasma detection kit, Biotool, Houston, TX, USA). Cell lines were maintained at 37 °C with 5% CO_2. Cell lines were validated by the Molecular Biology Service Center in the Barbara Davis Center for Diabetes.

In Vivo Angiogenesis Assessment: Dynamic contrast-enhanced magnetic resonance imaging (DCE-MRI).

Non-invasive measurements of tumor vascularity were performed on 2 sensitive CRC PDX models (CRC098 and 162) to measure treatment effects on angiogenesis. Mice were treated with cabozantinib and regorafenib and subjected to DCE-MRI (n = 4–8 tumors/group). DCE-MRI was done at baseline (prior to treatment), and on day 7 and day 28 (end of the treatment cycle). Briefly, the animals were anesthetized with an intraperitoneal injection of ketamine/xylazine (60/10 mg/kg) and a tail vein catheter (filled with 0.4 mmol/kg of MultiHance, gadobenate dimeglubine) was placed. The animal was positioned inside a warmed animal holder and inserted into the Bruker 4.7 Tesla MRI scanner. All images were acquired using a 36-mm volume receiver and transmitter coin and Bruker ParaVision v4.0 software. First, a fast tripilot was obtained for anatomical localization. Then, a series of fast gradient-echo (GRE) T1-weighted scans was obtained for total acquisition time of 5 minutes. After 30 seconds of image acquisition (precontrast), gadolinium (Gd) contrast was injected through the tail vein catheter. T1-weighted Gd-enhanced MRI scans were continuously taken for another 4.5 minutes. For each dynamic frame, the T1-signal voxel intensities were calculated for each lesion and blood vessel. A compartmental pharmacokinetic model, using SAAM program (version 2, University of Washington, Seattle, WA) and Bruker Advanced ParaVision v4.0, in which correlation of tissue clearance of Gd and transcapillary exchange between tumor and blood vessels, was constructed based on T1-signal curves. The volume transfer constants (K^{trans}) and the areas under the T1-intensity curves (AUC and IAUC), total and the first 60 seconds of enhancement, were reported as quantitative assessments of tumor perfusion and permeability of Gd uptake (23).

Measurement of glucose uptake by 18-Fluoro-deoxyglucose positron emission tomography (FDG-PET) following cabozantinib and regorafenib treatment.

FDG-PET studies were conducted on 2 CRC PDX models (CRC098 and 162) to determine whether treatment alters glucose uptake. The animals were scanned at baseline (prior to treatment) and on day 7 and 28 following treatment with cabozantinib or regorafenib. Mice were fasted for 4 hrs and injected via tail vein with 150 μCi (5.55 MBq) of ^{18}F-fluorodeoxyglucose (FDG, obtained through PetNet). Animals were then anesthetized with 2–2.5% isoflurane, placed onto a warming pad in the Siemens mouse holder and inserted into a Siemens Inveon μPET/CT scanner. All scans were performed using Siemens Inveon Acquisition Workplace software (IAW v1.5). First, a fast CT scan was performed for anatomical localization (270° rotation with 18 rotation steps; 2048 × 2048 field of view; 4 binning with 80kV and 450μA; 30 msec exposure time; low-medium magnification; 60 μm effective pixel size; 6 min total scan time). Then, the bed was moved into the μPET scanner. All PET scans were acquired in a double-sampling mode to improve spatial resolution (1.2 mm). PET/CT image fusion for precise anatomical identification of the regions of interest (ROI) was performed by Siemens Inveon Workstation Research (IWR v3.0) software. Regions of interest were manually drawn within the tumor lesions and total radioactivity of the ROI was determined (in kBq/mL). The SUV was calculated as described by our group and others (24, 25). All PET/CT scans were performed at the UCCC Animal Imaging Shared Resources (AISR, N. Serkova).

Gene pathway analysis by RNA Seq

Total RNA from cabozantinib treated CRC explants at day 3 of treatment was extracted using RNAeasy kit (Qiagen). RNA Seq was used to determine gene expression in tumors of control and treated mice. Raw expression values were obtained and normalized by the Affymetrix Power Tools based on a multi-array average. Multiple probe sets representing the same gene were collapsed by the maximum value. To assess pathways enriched in the control versus cabozantinib treated explants, we used the software version 2.0.13 obtained from the Broad Institute (http://www.broad.mit.edu/gsea). We used the pathways defined by the Kyoto Encyclopaedia of Genes and Genomes (KEGG) as the gene set (26). Gene set permutations were performed 1,000 times for each analysis. We used the nominal p-value and Normalized Enrichment Score obtained from gene set enrichment analysis (GSEA) to sort the pathways regulated in the cabozantinib treated groups. RNA seq data has been uploaded in the NCBI GEO repository database (GSE60939).

Immunoblotting

Control and treated tumor specimens (15 mg/tumor tissue) were homogenized using a Qiagen tissue lyser. Following 10 minutes on ice the lysed tissue was centrifuged at 16,000 g at 4°C for 10 min. Protein quantification in each sample was determined using the 660 Protein Assay kit (Thermo Fisher). A total of 50 μg of sample was electrophoresed on a precast 4–12% Bis-Tris gel (Life Technologies). Proteins were then transferred onto a nitrocellulose membrane using the iBlot transfer system (Life Technologies). Membranes were blocked for 1 hour at room temperature using 3% casein. After blocking, the membranes were probed with the following primary antibodies (1:1,000) overnight at 4°C

with rocking: (phosphorylated and total: MET, AKT, hexokinase, pyruvate dehydrogenase, ULK1, ATG3, Beclin, LC3, SQSTM/p62 and Actin (Cell Signaling Technologies). Following washing three times with TBST, the membranes were incubated for 1 h at room temperature with anti-rabbit IgG (H+L) (DyLight™ 800 Conjugate) secondary antibody at a final dilution of 1:15,000. Signal images were captured using the Odyssey Infrared Imaging System (Li-Cor).

Receptor tyrosine kinase array

Control and treated tumor specimens (15 mg/tumor tissue) were homogenized using a Qiagen tissue lyser and protein was quantitated using the 660 Protein Assay kit. After blocking the slides containing 39 antibodies/well (RTK array; Cell Signaling Technologies) for 15 minutes, 50 μg of protein were added to the slide and incubated overnight at 4°C with gentle rocking. The slides were then washed and detection antibody was added to the slide followed by DyLight 680VR–linked Streptavidin. Slide images were captured using the Odyssey Infrared Imaging System (Li-Cor) and were quantified using the Odyssey system software.

Autophagy

Treatment effects of cabozantinib, regorafenib, and crizotinib on autophagy were evaluated on the HCT116 and HT29 cell lines using the CYTO-ID® Autophagy Detection Kit (Enzo - ENZ-51031-K200). HCT116 or HT29 cells were plated in 96 black-walled plate at a concentration of 1,000 cells/well. After 24 hours, the cells were treated with cabozantinib (5 μM), regorafenib (5 μM), and crizotinib (1 μM). Following 24 hours of incubation, the cells were washed 2x times with 1x assay buffer and then incubated for 30 minutes with the CYTO-ID® Autophagy Detection reagent. After 30 minutes, the cells were washed 2 times with 1x assay buffer. The effects of treatment were evaluated on the IncuCyte™ ZOOM live cell imager using 488nm-excitable green fluorescent detection.

Treatment effects on apoptosis

Next, we performed *in vitro* combination studies with the autophagy inhibitors chloroquine and/or SBI-0206965 (ULK1 inhibitor) on the HCT116 and HT29 CRC cells. Cells were plated in 96 black-well plate at a concentration of 1,000 cells/well and incubated overnight to allow cells to adhere. After 24 hours, the media was removed and 100 ul of media containing IncuCyte™ Kinetic Caspase-3/7 Apoptosis Assay Reagent (Cat No 4440) was added to each well. Immediately after the cells were treated with cabozantinib (5 μM), SBI-0206965 (5 μM), chloroquine (10 μM), cabozantinib (5 μM) plus SBI-0206965 (5 μM) and cabozantinib (5 μM) plus chloroquine (10 μM). In addition, regorafenib (5 μM) or crizotinib (1 μM) were used as a single agent and in combination with SBI-0206965 (5 μM). Treatment effects on apoptosis were measured every 2 hours (total of 36–48 hours) on the IncuCyte™ ZOOM live cell imager.

Statistical analysis

An unpaired t-test was used to compare the tumor growth inhibition index (TGII) differences between cabozantinib and regorafenib. The TGII is a standardized measure of tumor growth,

which is calculated using the following formula: TGII = (tumor volume of TX on Day 28 – tumor volume of TX on Day 0)/(tumor volume of Con on Day 28 – tumor volume of Con on Day 0) × 100, where TX is the cabozantinib or regorafenib treated xenograft and CX is the control treated xenograft. The differences were considered significant when the p value was <0.05. All error bars are represented as the standard error of the mean (SEM). A paired t-test was used to examine the differences in [^{18}F]-FDG-PET uptake and Gd DCE-MRI uptake at baseline, day 7 and day 28. The differences were considered significant when the p value was <0.05. A one-way analysis of variance (ANOVA) was used to determine whether the means were significantly different between treatments with respect to autophagy and apoptosis. If the overall means were significantly different, we performed a pair-wise comparison. P values were adjusted using Tukey's method for multiple comparisons. SEM error bars were indicated for each value. All statistical analyses were performed using GraphPad Prism Software.

Results

Cabozantinib exhibits significantly greater anti-tumor effects when compared to regorafenib in CRC PDX mouse models

Cabozantinib demonstrated greater anti-tumor activity when compared to regorafenib in 7 out of 10 CRC explants tested (Figure 1a), with no difference in body weight of the animals between the groups (data not shown). A comparison of the combined TGII among the 10 total CRC explants revealed that cabozantinib treatment was significantly better than regorafenib at tumor growth inhibition (P=0.007) (Figure 1b). Supplemental Table 1 displays the patient characteristics as well as gene mutations for each CRC explant treated on this study. Next, we determined whether treatment differences differed with a constitutively active MET kinase cell line. A heterozygous knock-in of MET activating mutation Y1253D was introduced in the HCT116 cell line. As displayed in Figure 1c–e, both compounds demonstrated similar anti-tumor activity in the HCT116 parental cell line; however, cabozantinib exhibited significantly improved antitumor effects compared to regorafenib in the MET kinase active cell line.

Evaluation of cabozantinib and regorafenib on angiogenesis.

We next investigated the treatment effects of regorafenib and cabozantinib on angiogenesis using DCE-MRI. Cabozantinib treatment significantly reduced tumor vascularity in CRC098 and CRC162 after 28 days of treatment compared to baseline (Supplemental Table 2 and Figure 2). Evaluation of VEGFR2 and TIE2 revealed a decrease in activation as early as 4 hours, which was sustained for 7 days after cabozantinib treatment (Figure 2b–d). Regorafenib treatment of CRC098 also exhibited a decrease in vascularity (Supplemental Table 2) as well as in the activation of VEGFR2 and TIE2 (Supplemental Figure 1). In contrast, no changes in vascularity were observed in CRC162 after regorafenib treatment (Supplemental Table 2).

Reduction of PI3K/AKT/mTOR signalling pathway following cabozantinib treatment.

RTK activation plays an essential role in facilitating extracellular signals to downstream targets including the PI3K signalling pathway. Phospho-protein levels involved in the PI3K/

mTOR signalling pathway were significantly reduced after cabozantinib treatment including PI3K, PDK1, AKT, mTOR, Rictor, Raptor, and S6K1/2 (Figure 3a). In addition, analysis of RTK activation by an antibody array revealed a decrease in the phosphorylation of MET, RET, and AXL, and a subsequent decrease in AKT and S6 after cabozantinib treatment in CRC098 and CRC162 (Figure 3b–g). A maximal decrease in activation was observed at 8 hours after treatment in CRC 098 and 162. Regorafenib did not demonstrate significantly reduced levels of pMET, pRET, pAXL, AKT, and pS6 in CRC098 or CRC162 (Supplemental Figure 2).

Examination of glucose uptake (18[F] FDG-PET) following cabozantinib treatment.

Upon observation that cabozantinib significantly reduced downstream effectors in the PI3K/AKT/mTOR signaling pathway, we hypothesized that cabozantinib may be an important modulator of tumor cell metabolism. Cabozantinib significantly reduced glucose uptake measured by [^{18}F]-FDG-PET at days 7 and 28 compared to baseline in the CRC098 and CRC162 explants (Figure 4a and Supplemental Table 3). Regorafenib did not significantly reduce glucose uptake in the CRC098 or 162.

Next, we performed a comprehensive pathway analysis aided by the KEGG database using RNA Seq post-cabozantinib treatment in the most sensitive explants (CRC020, 102, and 162). Significant decreases in pathways controlling glycolysis and the TCA cycle were observed (Supplemental Table 4). In addition, Western Blot analysis demonstrated downregulation of pyruvate dehydrogenase on days 7 and 28 following cabozantinib treatment in the CRC098 and CRC162 explants compared to control (Figure 4b). In contrast, no decrease in pyruvate dehydrogenase was observed after regorafenib treatment in CRC098 and 162 explants (Figure 4b).

Cabozantinib induces autophagy that may provide a mechanism for tumor cell survival.

Both glucose deprivation and PI3K/mTOR pathway inhibition have been shown to trigger autophagy (27). As shown above, we determined that cabozantinib significantly decreased glucose uptake as well as the PI3K/mTOR signaling pathway. Therefore, we investigated autophagy as an alternate metabolic pathway for cell survival *in vitro* following cabozantinib treatment. Increased protein expression of ATG3, LC3 and beclin-1 occurred as early as 7 days after cabozantinib treatment (Figure 5a). In addition, evaluation of CRC020 and CRC040 explants (both sensitive) showed a decrease in SQSTM1/p62 with cabozantinib treatment on days 7 and 28 (Figure 5b). No increase in ATG3, LC3A/B, and beclin1 in CRC098 and CRC162 were observed after regorafenib treatment, apart from a modest increase in LC3A/B in the CRC162 explant when considered with the actin loading control (Supplemental Figure 3).

Given that we observed a significant increase in autophagy following cabozantinib treatment, we examined whether combining an autophagy inhibitor with cabozantinib would enhance tumor cell death. First, the treatment effects on autophagy were evaluated *in vitro* using an autophagy kit (CYTO-ID® Autophagy Detection Kit) that monitors autophagic activity at the cellular level (28, 29). Twenty-four hours of treatment with cabozantinib significantly induced autophagy when compared to control and regorafenib treatment in the

HCT116 and HT29 cell lines (Figure 5c-d and supplemental figure 4). Next, we tested the combination of cabozantinib with the autophagy inhibitors SBI-0206965, an ULK1 inhibitor, and chloroquine. Using a caspase 3/7 fluorescent reagent and IncuCyte live cell imager, we observed a striking increase in apoptosis in the HCT116 cells treated with SBI-0206965 plus cabozantinib and chloroquine plus cabozantinib over 48 hours (Figure 5E)(29). In contrast, no combinational effect was seen in the HCT116 cell line when treated with regorafenib (Figure 5F. Furthermore, while an increase in autophagy was observed using crizotinib, a potent MET inhibitor, a combinational effect was not seen with crizitonib plus SBI-020695 in the HCT116 and HT29 CRC cell lines (Supplemental Figure 4).

Discussion

We previously demonstrated that cabozantinib exerts potent anti-tumor effects in colorectal PDX models; 7 out of 10 CRC explants showed significantly superior anti-tumor effects, and 5 of the 9 cabozantinib sensitive CRC explants displayed tumor regression (18). In this study, using regorafenib (FDA approved for resistant advanced colorectal cancer) as a comparator, we showed that cabozantinib is superior in inhibiting tumor growth in CRC PDX models and mechanistic studies showed unique pharmacodynamic effects of cabozantinib in this model. Only 1 of the 10 CRC explants, CRC036, showed a trend toward improved anti-tumor effect with regorafenib. Dosages used in the PDX models were chosen to approximate plasma drug exposures within the pharmacodynamic range achievable in humans (20, 30–34).

Preclinical studies have demonstrated the role of MET in facilitating anti-VEGF treatment resistance (6, 7, 35). As with VEGF activation, MET signalling has been shown to be a potent inducer of endothelial angiogenesis (36–38). While MET and the VEGF receptor family are not known to interact with or phosphorylate one another, these kinases synergistically activate similar downstream intermediates including FAK, MAPK, and AKT (12). Data from preclinical studies have also shown that MET activation promotes angiogenesis through other common signalling intermediates such as SRC homology 2 domain-containing proteins (SHCs). *In vivo* and *in vitro* studies have demonstrated reduction in angiogenesis leading to apoptosis with MET inhibition (18). In this study, cabozantinib showed a significant decrease in tumor vascularity compared to regorafenib as measured by DCE-MRI, a technique that has been shown to correlate with tumor vascularity and angiogenesis in preclinical and clinical studies (39–41). While cabozantinib and regorafenib both have anti-angiogenic properties via VEGFR2 inhibition, dual MET and VEGFR2 inhibition may explain the observed differences in treatment effects in tumor vascularity. In addition, a near immediate and sustained decrease in protein expression of angiogenic mediators VEGFR2 and TIE2 was also observed to a larger degree with cabozantinib.

Enhanced antitumor effects of cabozantinib were also displayed in the constitutively activated MET kinase cell line. Physiologic activation of MET through HGF ligand binding elicits a complex network of downstream signalling that affects cell cycle regulation, cell survival, and cell migration and adhesion mainly through the PI3K/AKT/mTOR, Src, and RAS/MEK pathways (42, 43). Aberrant MET activation after exposure to anti-VEGF

treatment leads to acquired resistance and induces an upregulation in crosstalk pathways responsible for cell survival, angiogenesis, and EMT (44–46). In addition to reducing VEGFR2 and TIE2 levels and tumor vascularization, pathway analysis showed that many components involved in the PI3K/AKT/mTOR pathway were significantly decreased with cabozantinib treatment, including PI3K, PDK1, AKT, mTOR, Rictor, Raptor, and S6K1/2. This observed decrease in both tumor vascularity and activation of MET, RET, and AXL suggests that inhibition of multiple crosstalk pathways may abrogate acquired resistance observed with other anti-VEGF therapies.

The PI3K/AKT/mTOR pathway regulates cellular metabolism through multiple downstream targets including hypoxia inducible factor-1 (HIF-1), which is involved in glucose metabolism, and ULK-1, which is involved in autophagy (47, 48). Inhibition of the PI3K/AKT/mTOR pathway leads to disruption of glucose uptake. This was confirmed with cabozantinib treatment, where both a significant decrease in PI3K/AKT/mTOR mediators and glucose uptake measured by [^{18}F]-FDG-PET was observed. In contrast, a change in glucose uptake was not significantly altered after regorafenib treatment. Further investigation demonstrated a significant decrease in pyruvate metabolism and gene analysis of the TCA cycle with cabozantinib treatment compared to baseline, which was also not observed after regorafenib treatment. These alterations suggest that inhibition of the PI3K/AKT/mTOR pathway leads to a decrease in glucose metabolism and glycolytic inhibition with cabozantinib treatment.

Glucose deprivation and inhibition of PI3K/AKT/mTOR pathway has previously been shown to induce autophagy in preclinical studies (27, 48, 49). Protein expression of key enzymes in autophagy including ATG3, LC3, and beclin1 increased during cabozantinib treatment compared to baseline. These changes were not observed after regorafenib treatment. Under normal conditions, basal levels of autophagy are usually low and are restricted to maintaining important cellular functions. However, during times of nutrient deprivation and hypoxic conditions, autophagy is upregulated to promote metabolic homeostasis and survival of cells (50–53). Pharmacological inhibition of the PI3K/AKT/mTOR pathway enhances autophagy by inhibiting mTOR-mediated activation of the ULK1 complex, leading to subsequent lysosomal degradation of cellular components for ATP energy (Supplemental Figure 6) (54, 55). Together with glycolytic inhibition and upregulation of components involved in autophagy, an increase in autophagy occurred during cabozantinib treatment in the HCT116 and HT29 CRC cell lines. Using an autophagy detection kit, significant induction of autophagy was observed *in vitro* after 24 hours of cabozantinib compared to regorafenib and control. These results further support the concept that multi-kinase inhibition with cabozantinib, specifically the PI3K/AKT/mTOR pathway through MET inhibition, elicits a transition from glycosis-dependent to autophagy-dependent metabolism as a means for continued cell survival.

These findings are consistent with previously published data demonstrating autophagy as a mechanism for acquired resistance to certain anti-cancer therapies (56). Striking *in vitro* effects of combination treatment using anti-autophagy agents SBI-0206965, an ULK1 inhibitor, or chloroquine plus cabozantinib revealed increased apoptotic marker caspase 3/7 fluorescent assay. Regorafenib in combination with these anti-autophagy agents did not

reveal an increase in caspase 3/7 activity. While crizotinib, a potent MET inhibitor, produced similar MET suppression compared to cabozantinib, there was no increase in autophagy when SBI-020695 was added to crizotinib. These findings suggest that there are multiple crosstalk pathways that allow ongoing glycolysis in the presence of MET inhibition. However, multiple kinase inhibition as seen with cabozantinib interrupts crosstalk as an escape mechanism for ongoing glycolysis and leads to induction of autophagy. Combining an anti-autophagy agent with cabozantinib confirmed this idea as both combinations with SBI-020695 and chloroquine augmented apoptotic response compared to baseline and single agent treatment in the HCT116 and HT29 cell lines.

Our results show that cabozantinib has superior anti-tumor effects compared to regorafenib *in vitro* and *in vivo* using CRC explant models. Dual inhibition of MET and VEGFR2 act synergistically to potentiate anti-angiogenic response by inhibiting multiple cross-talk pathways including PI3K/AKT/mTOR. The inhibition of multiple kinase pathways produces a change in metabolism from glycolysis to autophagy, serving as a method for acquired resistance and cell survival during cabozantinib treatment. Combination of cabozantinib plus an anti-autophagy agent increased apoptosis in the HCT116 and HT29 CRC cell lines. These findings warrant further investigation of cabozantinib in CRC and combination approaches targeting autophagy. A clinical trial is currently under development to study the efficacy of cabozantinib in patients with refractory mCRC.

Supplementary Material

Refer to Web version on PubMed Central for supplementary material.

Acknowledgements

This work was supported by grant 1R01CA152303 (W.A. Messersmith), as well as in part by the Shared Resource of the University of Colorado Cancer Center P30CA046934 (W.A. Messersmith). Support was also received by Exelixis (TP). We also thank the patients who consented to allow their tumor tissue to be used in these experiments.

Financial Support:

This work was supported by the NIH (1R01CA152303–01) and the University of Colorado Cancer Center Shared Resource (P30CA046934)

References:

1. U.S. Cancer Statistics Working Group. United States Cancer Statistics: 1999–2012 Incidence and Mortality Web-based Report. Atlanta: U.S. Department of Health and Human Services, Centers for Disease Control and Prevention and National Cancer Institute; 2015 Available at: http://www.cdc.gov/uscs.
2. Grothey A, Van Cutsem E, Sobrero A, Siena S, Falcone A, Ychou M, et al. Regorafenib monotherapy for previously treated metastatic colorectal cancer (CORRECT): an international, multicentre, randomised, placebo-controlled, phase 3 trial. Lancet (London, England). 2013;381(9863):303–12. Epub 2012/11/28. doi: 10.1016/s0140-6736(12)61900-x. PubMed PMID: . [PubMed: 23177514]
3. Mayer RJ, Van Cutsem E, Falcone A, Yoshino T, Garcia-Carbonero R, Mizunuma N, et al. Randomized trial of TAS-102 for refractory metastatic colorectal cancer. The New England journal of medicine. 2015;372(20):1909–19. Epub 2015/05/15. doi: 10.1056/NEJMoa1414325. PubMed PMID: . [PubMed: 25970050]

4. Ferrara N The role of VEGF in the regulation of physiological and pathological angiogenesis. Exs. 2005(94):209–31. Epub 2004/12/25. PubMed PMID: . [PubMed: 15617481]
5. Hurwitz H Integrating the anti-VEGF-A humanized monoclonal antibody bevacizumab with chemotherapy in advanced colorectal cancer. Clinical colorectal cancer. 2004;4 Suppl 2:S62–8. Epub 2004/10/14. PubMed PMID: . [PubMed: 15479481]
6. Shojaei F, Simmons BH, Lee JH, Lappin PB, Christensen JG. HGF/c-Met pathway is one of the mediators of sunitinib-induced tumor cell type-dependent metastasis. Cancer letters. 2012;320(1): 48–55. Epub 2012/01/25. doi: 10.1016/j.canlet.2012.01.026. PubMed PMID: . [PubMed: 22269210]
7. Paez-Ribes M, Allen E, Hudock J, Takeda T, Okuyama H, Vinals F, et al. Antiangiogenic therapy elicits malignant progression of tumors to increased local invasion and distant metastasis. Cancer cell. 2009;15(3):220–31. Epub 2009/03/03. doi: 10.1016/j.ccr.2009.01.027. PubMed PMID: ; PubMed Central PMCID: PMCPMC2874829. [PubMed: 19249680]
8. Ebos JM, Lee CR, Cruz-Munoz W, Bjarnason GA, Christensen JG, Kerbel RS. Accelerated metastasis after short-term treatment with a potent inhibitor of tumor angiogenesis. Cancer cell. 2009;15(3):232–9. Epub 2009/03/03. doi: 10.1016/j.ccr.2009.01.021. PubMed PMID: ; PubMed Central PMCID: PMCPMC4540346. [PubMed: 19249681]
9. Gherardi E, Birchmeier W, Birchmeier C, Vande Woude G. Targeting MET in cancer: rationale and progress. Nature reviews Cancer. 2012;12(2):89–103. Epub 2012/01/25. doi: 10.1038/nrc3205. PubMed PMID: . [PubMed: 22270953]
10. Takeuchi H, Bilchik A, Saha S, Turner R, Wiese D, Tanaka M, et al. c-MET expression level in primary colon cancer: a predictor of tumor invasion and lymph node metastases. Clinical cancer research : an official journal of the American Association for Cancer Research. 2003;9(4):1480–8. Epub 2003/04/10. PubMed PMID: . [PubMed: 12684423]
11. Pennacchietti S, Michieli P, Galluzzo M, Mazzone M, Giordano S, Comoglio PM. Hypoxia promotes invasive growth by transcriptional activation of the met protooncogene. Cancer cell. 2003;3(4):347–61. Epub 2003/05/03. PubMed PMID: . [PubMed: 12726861]
12. Sulpice E, Ding S, Muscatelli-Groux B, Berge M, Han ZC, Plouet J, et al. Cross-talk between the VEGF-A and HGF signalling pathways in endothelial cells. Biology of the cell / under the auspices of the European Cell Biology Organization. 2009;101(9):525–39. Epub 2009/03/14. doi: 10.1042/bc20080221. PubMed PMID: . [PubMed: 19281453]
13. Gerritsen ME, Tomlinson JE, Zlot C, Ziman M, Hwang S. Using gene expression profiling to identify the molecular basis of the synergistic actions of hepatocyte growth factor and vascular endothelial growth factor in human endothelial cells. British journal of pharmacology. 2003;140(4):595–610. Epub 2003/09/25. doi: 10.1038/sj.bjp.0705494. PubMed PMID: ; PubMed Central PMCID: PMCPMC1574080. [PubMed: 14504135]
14. Bottaro DP, Liotta LA. Cancer: Out of air is not out of action. Nature. 2003;423(6940):593–5. Epub 2003/06/06. doi: 10.1038/423593a. PubMed PMID: . [PubMed: 12789320]
15. Bladt F, Riethmacher D, Isenmann S, Aguzzi A, Birchmeier C. Essential role for the c-met receptor in the migration of myogenic precursor cells into the limb bud. Nature. 1995;376(6543):768–71. Epub 1995/08/31. doi: 10.1038/376768a0. PubMed PMID: . [PubMed: 7651534]
16. Elisei R, Schlumberger MJ, Muller SP, Schoffski P, Brose MS, Shah MH, et al. Cabozantinib in progressive medullary thyroid cancer. Journal of clinical oncology : official journal of the American Society of Clinical Oncology. 2013;31(29):3639–46. Epub 2013/09/05. doi: 10.1200/jco.2012.48.4659. PubMed PMID: ; PubMed Central PMCID: PMCPMC4164813. [PubMed: 24002501]
17. Choueiri TK, Escudier B, Powles T, Mainwaring PN, Rini BI, Donskov F, et al. Cabozantinib versus Everolimus in Advanced Renal-Cell Carcinoma. The New England journal of medicine. 2015;373(19):1814–23. Epub 2015/09/26. doi: 10.1056/NEJMoa1510016. PubMed PMID: . [PubMed: 26406150]
18. Song EK, Tai WM, Messersmith WA, Bagby S, Purkey A, Quackenbush KS, et al. Potent antitumor activity of cabozantinib, a c-MET and VEGFR2 inhibitor, in a colorectal cancer patient-derived tumor explant model. International journal of cancer Journal international du cancer. 2015;136(8):1967–75. Epub 2014/09/23. doi: 10.1002/ijc.29225. PubMed PMID: ; PubMed Central PMCID: PMCPMC4323738. [PubMed: 25242168]

19. Tentler JJ, Tan AC, Weekes CD, Jimeno A, Leong S, Pitts TM, et al. Patient-derived tumour xenografts as models for oncology drug development. Nature reviews Clinical oncology. 2012;9(6):338–50. Epub 2012/04/18. doi: 10.1038/nrclinonc.2012.61. PubMed PMID: ; PubMed Central PMCID: PMCPMC3928688. [PubMed: 22508028]
20. Wilhelm SM, Dumas J, Adnane L, Lynch M, Carter CA, Schütz G, et al. Regorafenib (BAY 73–4506): A new oral multikinase inhibitor of angiogenic, stromal and oncogenic receptor tyrosine kinases with potent preclinical antitumor activity. International Journal of Cancer. 2011;129(1): 245–55. doi: 10.1002/ijc.25864. [PubMed: 21170960]
21. Huynh H, Ong R, Zopf D. Antitumor activity of the multikinase inhibitor regorafenib in patient-derived xenograft models of gastric cancer. Journal of Experimental & Clinical Cancer Research. 2015;34(1):132. doi: 10.1186/s13046-015-0243-5. [PubMed: 26514182]
22. Daudigeos-Dubus E, Le Dret L, Lanvers-Kaminsky C, Bawa O, Opolon P, Vievard A, et al. Regorafenib: Antitumor Activity upon Mono and Combination Therapy in Preclinical Pediatric Malignancy Models. PloS one. 2015;10(11):e0142612 Epub 2015/11/26. doi: 10.1371/journal.pone.0142612. PubMed PMID: ; PubMed Central PMCID: PMCPMC4658168. [PubMed: 26599335]
23. Longo DL, Dastru W, Consolino L, Espak M, Arigoni M, Cavallo F, et al. Cluster analysis of quantitative parametric maps from DCE-MRI: application in evaluating heterogeneity of tumor response to antiangiogenic treatment. Magnetic resonance imaging. 2015;33(6):725–36. Epub 2015/04/04. doi: 10.1016/j.mri.2015.03.005. PubMed PMID: . [PubMed: 25839393]
24. Serkova NJ, Garg K, Bradshaw-Pierce EL. Oncologic imaging end-points for the assessment of therapy response. Recent patents on anti-cancer drug discovery. 2009;4(1):36–53. Epub 2009/01/20. PubMed PMID: . [PubMed: 19149687]
25. Dandekar M, Tseng JR, Gambhir SS. Reproducibility of 18F-FDG microPET studies in mouse tumor xenografts. Journal of nuclear medicine : official publication, Society of Nuclear Medicine. 2007;48(4):602–7. Epub 2007/04/03. PubMed PMID: ; PubMed Central PMCID: PMCPMC4161128. [PubMed: 17401098]
26. Kanehisa M, Furumichi M, Tanabe M, Sato Y, Morishima K. KEGG: new perspectives on genomes, pathways, diseases and drugs. Nucleic acids research. 2016. doi: 10.1093/nar/gkw1092.
27. Yang X, Niu B, Wang L, Chen M, Kang X, Wang L, et al. Autophagy inhibition enhances colorectal cancer apoptosis induced by dual phosphatidylinositol 3-kinase/mammalian target of rapamycin inhibitor NVP-BEZ235. Oncology letters. 2016;12(1):102–6. Epub 2016/06/28. doi: 10.3892/ol.2016.4590. PubMed PMID: ; PubMed Central PMCID: PMCPMC4906634. [PubMed: 27347108]
28. Chan LL, Shen D, Wilkinson AR, Patton W, Lai N, Chan E, et al. A novel image-based cytometry method for autophagy detection in living cells. Autophagy. 2012;8(9):1371–82. doi: 10.4161/auto.21028. PubMed PMID: ; PubMed Central PMCID: PMCPMC3442883. [PubMed: 22895056]
29. Egan DF, Chun MG, Vamos M, Zou H, Rong J, Miller CJ, et al. Small Molecule Inhibition of the Autophagy Kinase ULK1 and Identification of ULK1 Substrates. Mol Cell. 2015;59(2):285–97. doi: 10.1016/j.molcel.2015.05.031. PubMed PMID: ; PubMed Central PMCID: PMCPMC4530630. [PubMed: 26118643]
30. Nguyen HM, Ruppender N, Zhang X, Brown LG, Gross TS, Morrissey C, et al. Cabozantinib inhibits growth of androgen-sensitive and castration-resistant prostate cancer and affects bone remodeling. PloS one. 2013;8(10):e78881 Epub 2013/11/10. doi: 10.1371/journal.pone.0078881. PubMed PMID: ; PubMed Central PMCID: PMCPMC3808282. [PubMed: 24205338]
31. Sennino B, Ishiguro-Oonuma T, Wei Y, Naylor RM, Williamson CW, Bhagwandin V, et al. Suppression of tumor invasion and metastasis by concurrent inhibition of c-Met and VEGF signaling in pancreatic neuroendocrine tumors. Cancer discovery. 2012;2(3):270–87. Epub 2012/05/16. doi: 10.1158/2159-8290.cd-11-0240. PubMed PMID: ; PubMed Central PMCID: PMCPMC3354652. [PubMed: 22585997]
32. Bentzien F, Zuzow M, Heald N, Gibson A, Shi Y, Goon L, et al. In vitro and in vivo activity of cabozantinib (XL184), an inhibitor of RET, MET, and VEGFR2, in a model of medullary thyroid cancer. Thyroid : official journal of the American Thyroid Association. 2013;23(12):1569–77. Epub 2013/05/28. doi: 10.1089/thy.2013.0137. PubMed PMID: ; PubMed Central PMCID: PMCPMC3868259. [PubMed: 23705946]

33. Graham TJ, Box G, Tunariu N, Crespo M, Spinks TJ, Miranda S, et al. Preclinical evaluation of imaging biomarkers for prostate cancer bone metastasis and response to cabozantinib. Journal of the National Cancer Institute. 2014;106(4):dju033 Epub 2014/03/19. doi: 10.1093/jnci/dju033. PubMed PMID: . [PubMed: 24634505]
34. Huynh H, Ong R, Zopf D. Antitumor activity of the multikinase inhibitor regorafenib in patient-derived xenograft models of gastric cancer. Journal of experimental & clinical cancer research : CR. 2015;34:132 Epub 2015/10/31. doi: 10.1186/s13046-015-0243-5. PubMed PMID: ; PubMed Central PMCID: PMCPMC4625870. [PubMed: 26514182]
35. Ebos JM, Lee CR, Kerbel RS. Tumor and host-mediated pathways of resistance and disease progression in response to antiangiogenic therapy. Clinical cancer research : an official journal of the American Association for Cancer Research. 2009;15(16):5020–5. Epub 2009/08/13. doi: 10.1158/1078-0432.ccr-09-0095. PubMed PMID: ; PubMed Central PMCID: PMCPMC2743513. [PubMed: 19671869]
36. Abounader R, Laterra J. Scatter factor/hepatocyte growth factor in brain tumor growth and angiogenesis. Neuro-oncology. 2005;7(4):436–51. Epub 2005/10/11. doi: 10.1215/s1152851705000050. PubMed PMID: ; PubMed Central PMCID: PMCPMC1871724. [PubMed: 16212809]
37. Bussolino F, Di Renzo MF, Ziche M, Bocchietto E, Olivero M, Naldini L, et al. Hepatocyte growth factor is a potent angiogenic factor which stimulates endothelial cell motility and growth. The Journal of cell biology. 1992;119(3):629–41. Epub 1992/11/01. PubMed PMID: ; PubMed Central PMCID: PMCPMC2289675. [PubMed: 1383237]
38. Grant DS, Kleinman HK, Goldberg ID, Bhargava MM, Nickoloff BJ, Kinsella JL, et al. Scatter factor induces blood vessel formation in vivo. Proceedings of the National Academy of Sciences of the United States of America. 1993;90(5):1937–41. Epub 1993/03/01. PubMed PMID: ; PubMed Central PMCID: PMCPMC45995. [PubMed: 7680481]
39. Yeo DM, Oh SN, Jung CK, Lee MA, Oh ST, Rha SE, et al. Correlation of dynamic contrast-enhanced MRI perfusion parameters with angiogenesis and biologic aggressiveness of rectal cancer: Preliminary results. Journal of magnetic resonance imaging : JMRI. 2015;41(2):474–80. Epub 2014/01/01. doi: 10.1002/jmri.24541. PubMed PMID: . [PubMed: 24375840]
40. Kim SH, Lee HS, Kang BJ, Song BJ, Kim HB, Lee H, et al. Dynamic Contrast-Enhanced MRI Perfusion Parameters as Imaging Biomarkers of Angiogenesis. PloS one. 2016;11(12):e0168632 Epub 2016/12/31. doi: 10.1371/journal.pone.0168632. PubMed PMID: ; PubMed Central PMCID: PMCPMC5201289. [PubMed: 28036342]
41. Ma L, Xu X, Zhang M, Zheng S, Zhang B, Zhang W, et al. Dynamic contrast-enhanced MRI of gastric cancer: Correlations of the pharmacokinetic parameters with histological type, Lauren classification, and angiogenesis. Magnetic resonance imaging. 2016;37:27–32. Epub 2016/11/15. doi: 10.1016/j.mri.2016.11.004. PubMed PMID: . [PubMed: 27840273]
42. Birchmeier C, Birchmeier W, Gherardi E, Vande Woude GF. Met, metastasis, motility and more. Nature reviews Molecular cell biology. 2003;4(12):915–25. Epub 2003/12/20. doi: 10.1038/nrm1261. PubMed PMID: . [PubMed: 14685170]
43. Lai AZ, Abella JV, Park M. Crosstalk in Met receptor oncogenesis. Trends in cell biology. 2009;19(10):542–51. Epub 2009/09/18. doi: 10.1016/j.tcb.2009.07.002. PubMed PMID: . [PubMed: 19758803]
44. Trusolino L, Bertotti A, Comoglio PM. MET signalling: principles and functions in development, organ regeneration and cancer. Nature reviews Molecular cell biology. 2010;11(12):834–48. Epub 2010/11/26. doi: 10.1038/nrm3012. PubMed PMID: . [PubMed: 21102609]
45. Schmidt L, Duh FM, Chen F, Kishida T, Glenn G, Choyke P, et al. Germline and somatic mutations in the tyrosine kinase domain of the MET proto-oncogene in papillary renal carcinomas. Nature genetics. 1997;16(1):68–73. Epub 1997/05/01. doi: 10.1038/ng0597-68. PubMed PMID: . [PubMed: 9140397]
46. Mosesson Y, Mills GB, Yarden Y. Derailed endocytosis: an emerging feature of cancer. Nature reviews Cancer. 2008;8(11):835–50. Epub 2008/10/25. doi: 10.1038/nrc2521. PubMed PMID: . [PubMed: 18948996]

47. Denko NC. Hypoxia, HIF1 and glucose metabolism in the solid tumour. Nature reviews Cancer. 2008;8(9):705–13. Epub 2009/01/15. doi: 10.1038/nrc2468. PubMed PMID: . [PubMed: 19143055]

48. Kim KW, Mutter RW, Cao C, Albert JM, Freeman M, Hallahan DE, et al. Autophagy for cancer therapy through inhibition of pro-apoptotic proteins and mammalian target of rapamycin signaling. The Journal of biological chemistry. 2006;281(48):36883–90. Epub 2006/09/29. doi: 10.1074/jbc.M607094200. PubMed PMID: . [PubMed: 17005556]

49. Din FV, Valanciute A, Houde VP, Zibrova D, Green KA, Sakamoto K, et al. Aspirin inhibits mTOR signaling, activates AMP-activated protein kinase, and induces autophagy in colorectal cancer cells. Gastroenterology. 2012;142(7):1504–15.e3. Epub 2012/03/13. doi: 10.1053/j.gastro.2012.02.050. PubMed PMID: ; PubMed Central PMCID: PMCPMC3682211. [PubMed: 22406476]

50. Feng Y, He D, Yao Z, Klionsky DJ. The machinery of macroautophagy. Cell Res. 2014;24(1):24–41. doi: 10.1038/cr.2013.168. PubMed PMID: ; PubMed Central PMCID: PMCPMC3879710. [PubMed: 24366339]

51. Jiang X, Overholtzer M, Thompson CB. Autophagy in cellular metabolism and cancer. J Clin Invest. 2015;125(1):47–54. doi: 10.1172/JCI73942. PubMed PMID: ; PubMed Central PMCID: PMCPMC4382242. [PubMed: 25654550]

52. Autophagy Thorburn A. and its effects: making sense of double-edged swords. PLoS Biol. 2014;12(10):e1001967. doi: 10.1371/journal.pbio.1001967. PubMed PMID: ; PubMed Central PMCID: PMCPMC4196727. [PubMed: 25313680]

53. Thorburn A, Thamm DH, Gustafson DL. Autophagy and cancer therapy. Mol Pharmacol. 2014;85(6):830–8. doi: 10.1124/mol.114.091850. PubMed PMID: ; PubMed Central PMCID: PMCPMC4014668. [PubMed: 24574520]

54. Jung CH, Ro SH, Cao J, Otto NM, Kim DH. mTOR regulation of autophagy. FEBS letters. 2010;584(7):1287–95. Epub 2010/01/20. doi: 10.1016/j.febslet.2010.01.017. PubMed PMID: ; PubMed Central PMCID: PMC2846630. [PubMed: 20083114]

55. Kim YC, Guan KL. mTOR: a pharmacologic target for autophagy regulation. J Clin Invest. 2015;125(1):25–32. Epub 2015/02/06. doi: 10.1172/JCI73939. PubMed PMID: ; PubMed Central PMCID: PMC4382265. [PubMed: 25654547]

56. Kroemer G, Marino G, Levine B. Autophagy and the integrated stress response. Mol Cell. 2010;40(2):280–93. doi: 10.1016/j.molcel.2010.09.023. PubMed PMID: ; PubMed Central PMCID: PMCPMC3127250. [PubMed: 20965422]

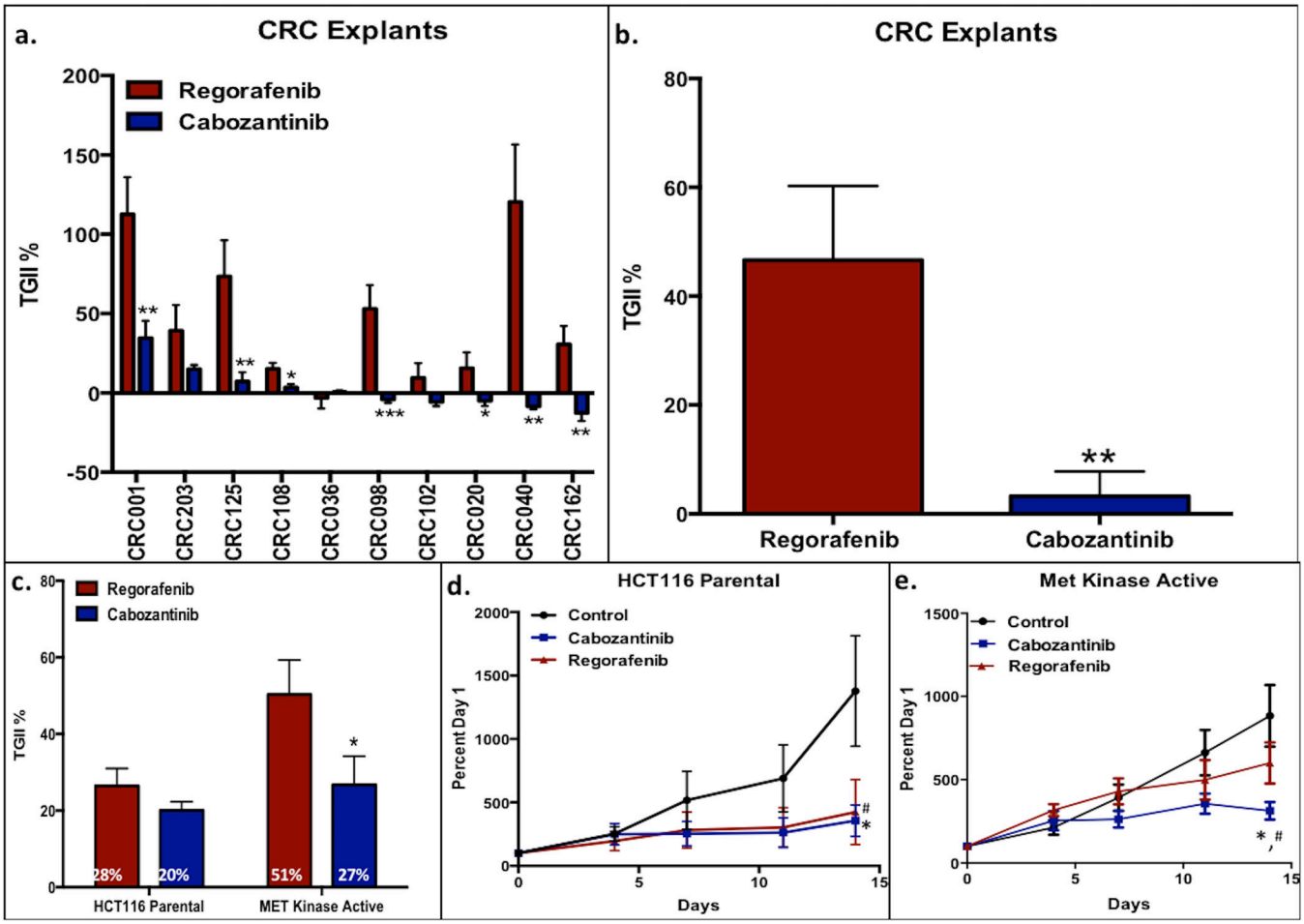

Figure 1:

Cabozantinib demonstrated significant antitumor effects compared to regorafenib in 7 out of 10 of the CRC explants; a) Five of the explants treated with cabozantinib showed tumor regression; b) significant tumor growth inhibition measured by TGII in 10 CRC explants with cabozantinib compared to regorafenib; c) cabozantinib maintained significant TGII in the engineered MET kinase active knock-in mutation Y1253D cell line compared to regorafenib *in vitro*; d, e) Percent growth curve of cabozantinib in the parental HCT116 cell line and the engineered MET kinase active cell line.

* $P < 0.05$, ** $P < 0.007$, *** $P < 0.001$; statistically significant difference in TGII with cabozantinib compared to regorafenib

# $p < 0.05$; statistically significant difference in TGII with cabozantinib compared to control

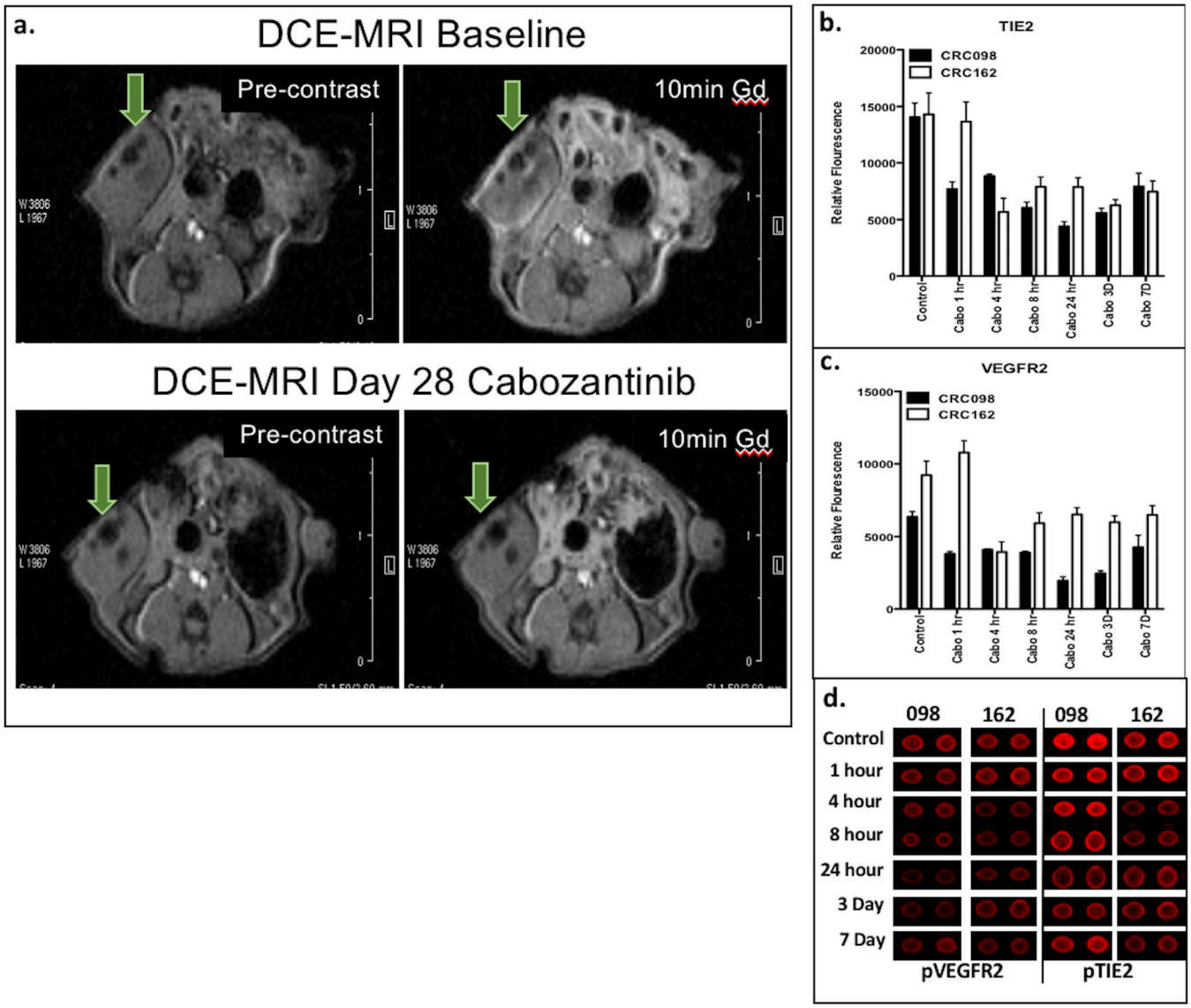

Figure 2:

a) DCE-MRI using Gd contrast revealed significant decrease in vascularity, measured in K^{trans} [min^{-1}], at day 28 of cabozantinib compared to baseline; b–d) RTK antibody assay using fluorescent analysis revealed decreased levels of TIE2 and VEGFR2 after 4 hours after treatment cabozantinib and were sustained through 7 days of treatment compared to control.

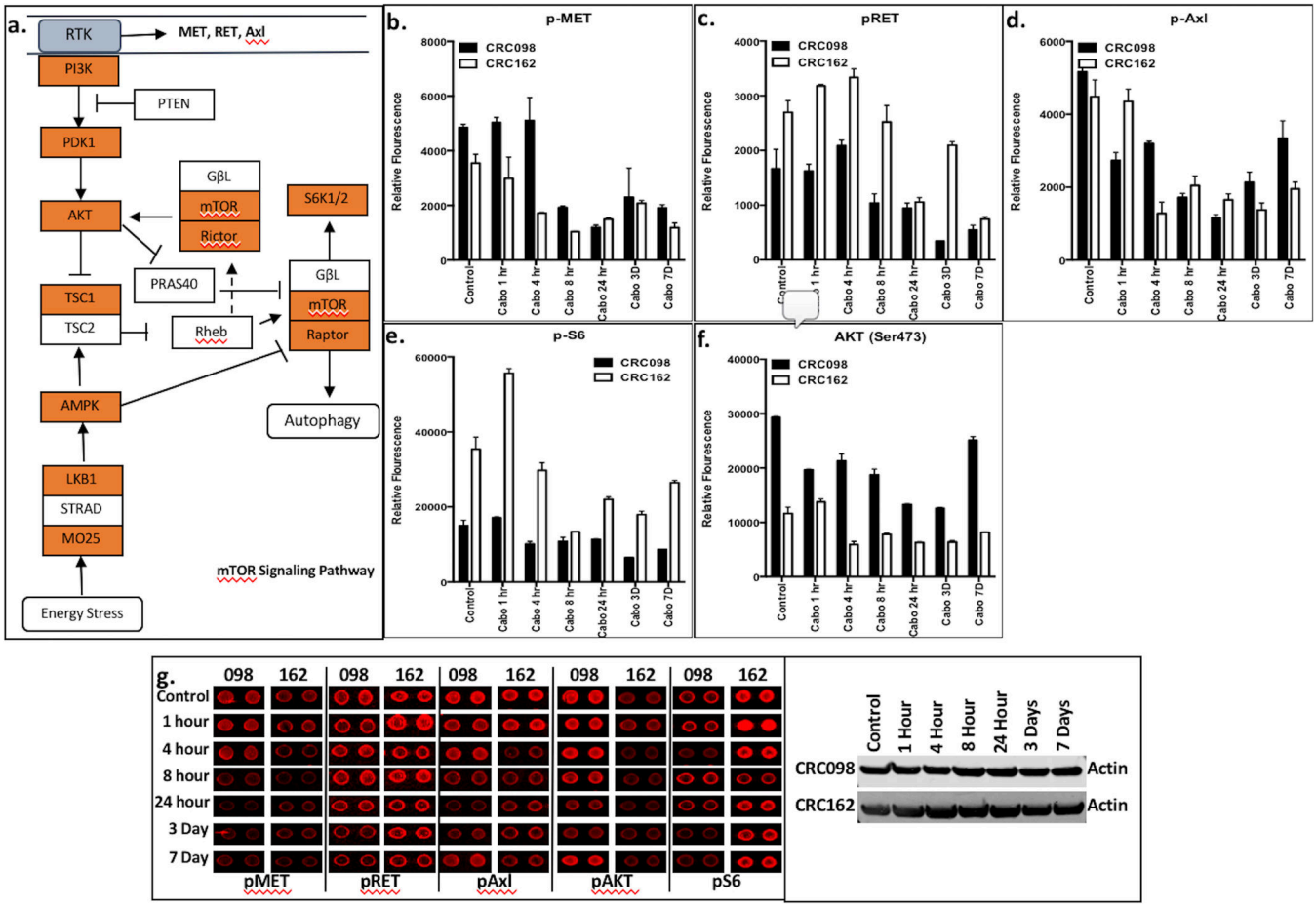

Figure 3:

Significant decrease in levels of activation of components in the PI3K/AKT/mTOR axis were observed using RTK antibody assay after cabozantinib treatment. a) Illustration of the enzymes with significant reduction in activation with cabozantinib are shown in red; b–f) significant reduction of phosphorylated MET, RET, AXL, AKT and S6 were observed with cabozantinib treatment after 7 days compared to control; g) RTK antibody fluorescent analysis showing decreased levels of the enzymes following 7 days of cabozantinib treatment in CRC098 and CRC162 explants.

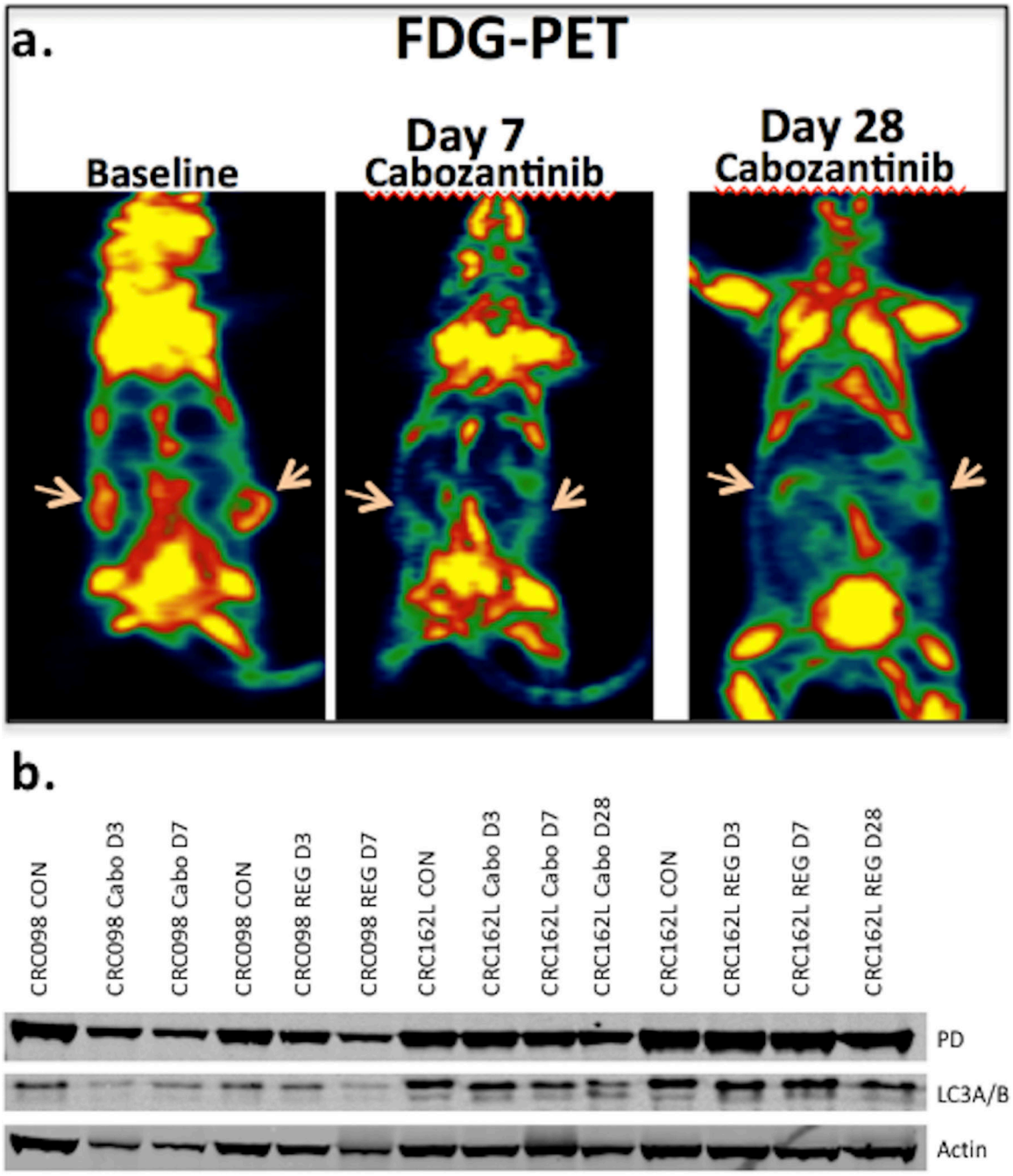

Figure 4:

a) Cabozantinib significantly reduced glucose uptake measured by [^{18}F] FDG-PET on day 7 and day 28 of treatment compared to baseline; b) Western Blot analysis revealed a decrease in protein expression of pyruvate dehydrogenase after cabozantinib treatment compared to regorafenib and control.

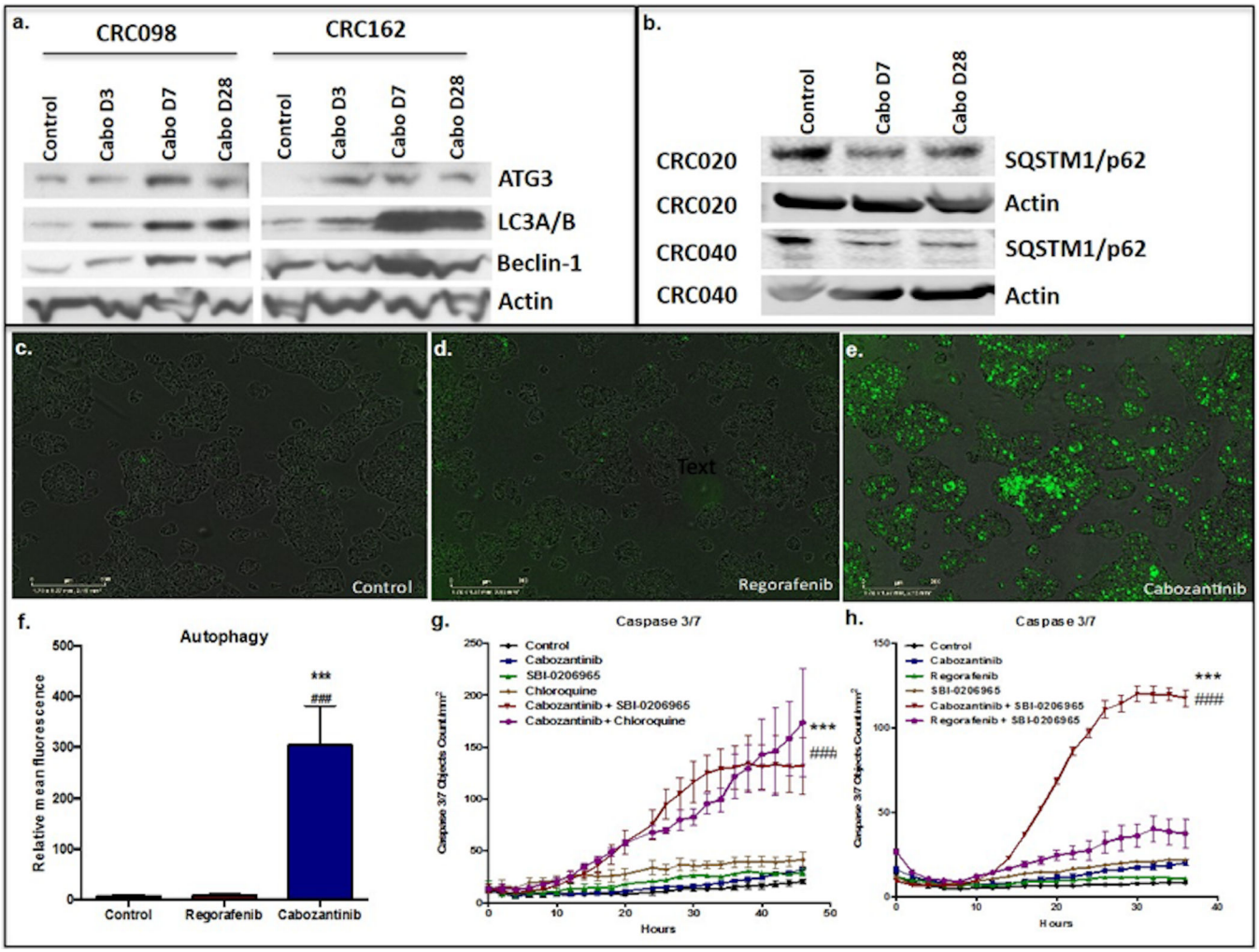

Figure 5:

a) Autophagy markers ATG3, LC3A/B, and beclin-1 increased after cabozantinib treatment in the CRC098 and CRC162 explant models; b) SQSTM1/p62 levels also increased after cabozantinib treatment in the CRC020 and CRC040 explant models; c–f) autophagy levels measured by CYTO-ID® Autophagy Detection Kit demonstrated a significant increase in autophagy after 24 hours of cabozantinib treatment compared to regorafenib and control; g) significant increase in levels of apoptosis measured by caspase 3/7 fluorescent assay after treatment with combination cabozantinib plus SBI-0206965, an ULK1 inhibitor, and cabozantinib plus chloroquine compared to control or single agent treatment; h) significant increase in levels of caspase 3/7 were not seen after combination treatment with regorafenib plus SBI-0206965 compared to control or single agent treatment.

*** Statistically significant increase in fluorescence after cabozantinib treatment compared to control

Statistically significant increase in fluorescence after cabozantinib treatment compared to regorafenib

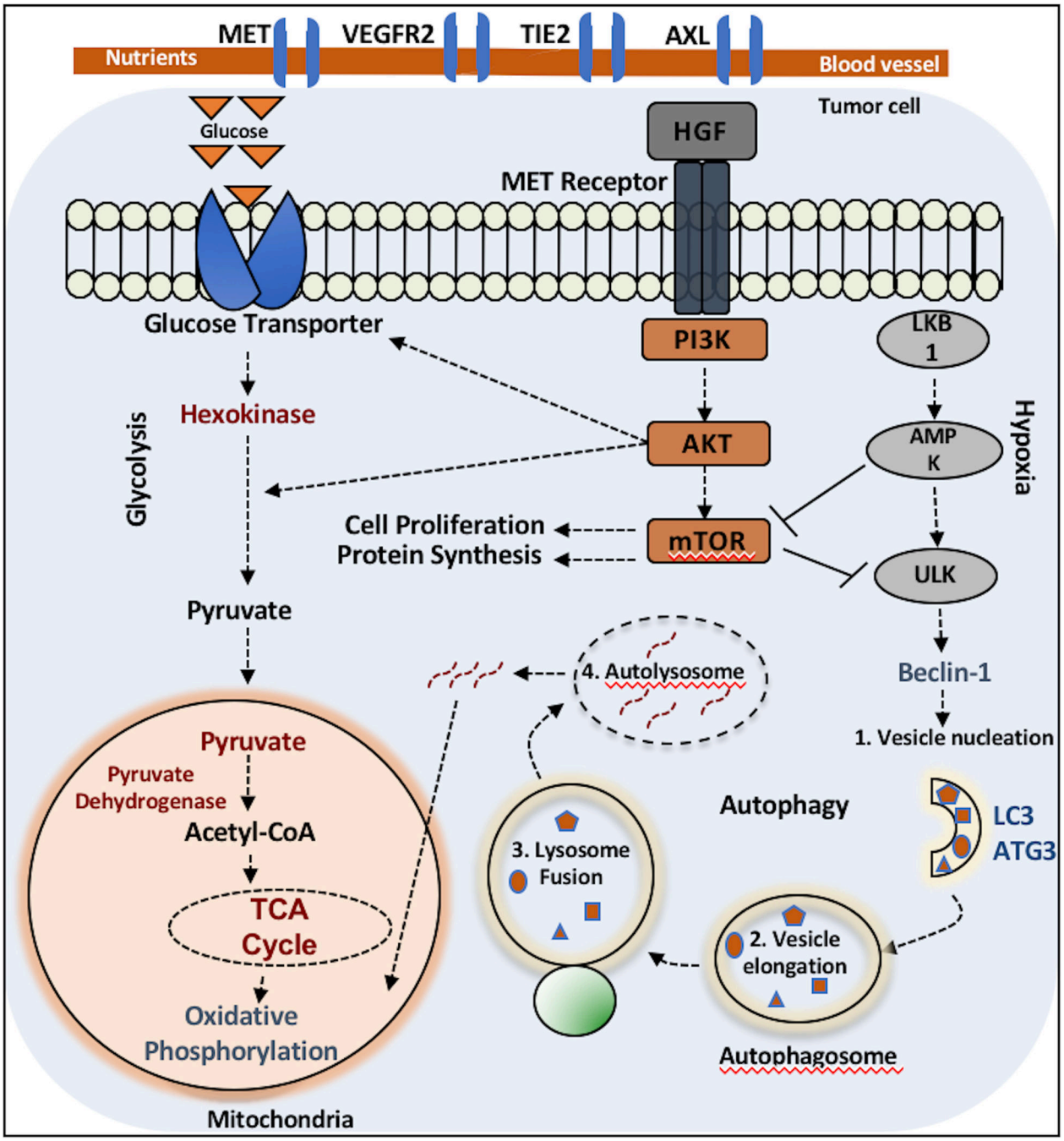

Figure 6:

In this illustration, potential mechanisms of tumor cell survival via crosstalk between components of the MET pathway, glycolysis, and autophagy are depicted. Basal levels of autophagy are typically low through mTOR inhibition of ULK1, a key enzyme in upregulation of autophagy, and glycolysis predominates as the main mechanism for ATP generation. Aberrant MET activation leads to upregulation of downstream effectors including components of the PI3K/AKT/mTOR pathway and glycolytic metabolism is maintained. Through blockade of MET and subsequent indirect activation of ULK1 through

the absence of negative feedback with mTOR inhibition, upregulation in autophagy occurs to maintain cellular homeostasis. A simplified canonical pathway of autophagy (steps 1–4) are shown.